Numerical simulation of wetting on a chemically textured surface with a large intrinsic contact angle ratio by the Lattice Boltzmann Method

Vincent Neyrand, Jean-Michel Bergheau, Stéphane Benayoun, Stéphane Valette

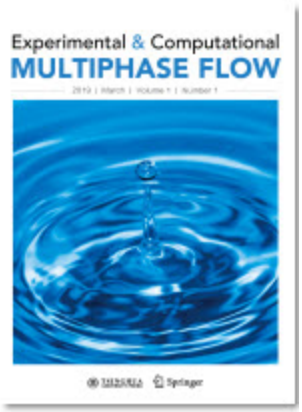

Numerical simulation of wetting on a chemically textured surface with a large intrinsic contact angle ratio by the Lattice Boltzmann Method

Journal:	*Experimental and Computational Multiphase Flow*
Manuscript ID	ECMF-2020-0038.R1
Manuscript Type:	Original Article
Date Submitted by the Author:	10-Sep-2020
Complete List of Authors:	NEYRAND, Vincent; Laboratoire de Tribologie et Dynamique des Systèmes Bergheau, Jean-Michel; Laboratoire de Tribologie et Dynamique des Systèmes Benayoun, Stéphane; Laboratoire de Tribologie et Dynamique des Systèmes Valette, Stéphane; Laboratoire de Tribologie et Dynamique des Systèmes
Keywords:	Wetting, Lattice Boltzmann Method, Chemically Textured Surfaces
Speciality:	Wetting

Numerical simulation of wetting on a chemically textured surface with a large intrinsic contact angle ratio by the Lattice Boltzmann Method

Vincent Neyrand[a,*], Jean-Michel Bergheau[b], Stéphane Benayoun[a], Stéphane Valette[a,*]

[a] *Univ Lyon, Ecole Centrale de Lyon, Laboratoire de Tribologie et Dynamique des Systèmes, UMR CNRS 5513, 36 avenue Guy de Collongue, 69134 Ecully Cedex, France*

[b] *Ecole Nationale d'Ingénieurs de Saint-Etienne, Laboratoire de Tribologie et Dynamique des Systèmes, UMR CNRS 5513, 58 Rue Jean Parot, 42100 Saint-Etienne, France*

[*]Corresponding authors. E-mail addresses: vincent.neyrand@ec-lyon.fr (V. Neyrand), stephane.valette@ec-lyon.fr (S. Valette)

Keywords: Wetting; Lattice Boltzmann Method; Chemically textured surfaces

Abstract

In the present paper, numerical sessile tests on chemically textured surfaces in 2D and 3D are simulated. The Lattice Boltzmann method coupled with pseudo potential model is used for the simulations. A modification of the fluid-solid potential is proposed using materials' intrinsic contact angle in order to control locally the wetting properties of a surface composed of different materials. The effect of the wetting potential and the wetting properties of chemically textured surfaces are discussed regarding to the simulations' results and compared to some common theoretical approaches of wetting on textured surfaces.

Introduction

In the nature, surfaces have roughness and/or coating patterns at small scale (Barthlott et al. 2017). Among them, some have shown interesting wetting properties like self-cleaning property for the lotus leaf (Zhang et al. 2016), drag reduction property for the shark skin (Zhang et al. 2011), optical functions (Niu et al. 2015), and so on. The development of surface texturing process over the last years allows the manufacturing of infinity of textures inspired by natural surfaces. As example, the reflectance principle of butterfly scales is copied to make a gas sensor (Jiang et al. 2014). Biomimicking the lotus effect to remove dust on solar cell panel is proposed in (Latthe et al. 2019). Being able to define precisely the behavior of a liquid in contact with a textured surface has a wide range of applications: transportation, coating, textiles, medical field and electronic devices (Bizi-Bandoki et al. 2011; Ge et al. 2014; Belaud et al. 2015; Mielczarek et al. 2016; Vera et al. 2017; Shin et al. 2018).

The first work trying to explain the phenomenon of wetting and its physical origin was done by Young in 1805 (Young 1805). He proposed to define wetting as the equilibrium of three domains: liquid, gas and solid. This representation of wetting was proposed for perfectly smooth and chemically homogeneous surfaces. He defines the term of contact angle (CA) which is still used to define wetting property of a surface. Subsequently, authors try to handle heterogeneities of surface. Wenzel (Wenzel 1936) proposed an upgrade of Young's law for rough surfaces and impregnated surface case. This case corresponds to a surface impregnated by liquid and it is called "Wenzel state". Cassie-Baxter (Cassie and Baxter 1944) proposed an upgrade of Young approach for a surface composed of different materials, which correspond to a chemical heterogeneous case. Cassie-Baxter extended this approach by replacing a material by gas to represent rough surfaces with gas trapped under the droplet. This case is called "Fakir state" or "Cassie state".

Those previous classical models have been discussed and improved these last years. Some experiments tend to show that the triple line, defined as the domain where liquid, gas and solid meet, has a role on droplet's spreading (Extrand 2003; Gao and McCarthy 2007). One common point of those studies is the use of contact angle hysteresis instead of Young's static contact angle (de Gennes 1985). The hysteresis of contact angle (CAH) has different origins (Erbil 2006) and it is a range of static angles for a motionless triple line. Texturing surfaces makes heterogeneities and consequently changes surface's CAH. The motion of the triple line has been the subject of small-scale studies (Choi et al. 2009; Dubov et al. 2012) showing the strong anisotropy of wetting on textured surfaces and exposing the difficulty to predict wetting behavior on textured surfaces.

Actually sessile test is used to measure CA of a liquid static droplet on a surface. However, manufactured textured surfaces can have patterns of 10 to 100µm (Pionnier et al. 2018; Divin-

Mariotti et al. 2019). At this scale, classical sessile test cannot measure exactly the position of the triple line and the impregnation rate in porosities. Moreover, the sessile test provides a static measurement so spreading rate can't be measured. Thus, to avoid those experimental limitations a numerical simulation tool has been developed. In addition to anticipating spreading on a surface, simulating wetting can lead to a better understanding of spreading mechanisms that are a source of disagreement in the literature (Erbil 2014). Various approaches are proposed in literature and summarized in (Sui et al. 2014). Authors combine computational fluid dynamics (CFD) and interface tracking method. Interface tracking methods allow the capture of the position of the fluid-fluid interface during spreading process and provide CA measurement (Sui et al. 2014). Fluid-fluid interface tracking methods are various. They can be separated in two categories: sharp interface or continuous interfaces. Volume-of-fluid (VOF) (Renardy et al. 2001; Zhang et al. 2017), level-set (LS) (Sussman et al. 1999; Spelt 2005; Solomenko et al. 2017; Bruchon et al. 2018) and front-tracking (Unverdi and Tryggvason 1992) are common sharp interface method. Diffuse interface (DI) (Cahn and Hilliard 1958; Yue and Feng 2011) is a continuous interface method. Continuous interface method is interesting in some cases because it is possible to simulate a multi-component or multi-phase system with a transition of fluids properties.

The simulation method chosen for this article is lattice Boltzmann method (Benzi et al. 1992) coupled with multi-component model (Shan and Chen 1994) because it allows to handle very easily all forms of solids and fluid-solid interactions without significant impact on the computation time. In addition, the computation time is low for this method because it can be parallelized on GPU. Lattice Boltzmann Method has been used for wetting simulation (Huang et al. 2007; Kubiak et al. 2011; Gong et al. 2017; Pravinraj and Patrikar 2017) and gives interesting results for both chemically and topographical textured surfaces. In the present research work, the simulation on chemically textured surface is tested and a fluid-solid potential computation is proposed. Section 1 presents the numerical method and its application to wetting studies. Section 2 exposes the results of validation tests. Section 3 and 4 present results for 2D and 3D simulation on flat and chemically textured surfaces for various textured patterns and their comparison with classical theoretical approaches to wetting on textured surfaces.

1. Numerical Method

1.1 Lattice Boltzmann Method

The lattice Boltzmann method relies on Boltzmann equations at mesoscopic scale to define the behavior of a fluid (Benzi et al. 1992). In a phase-space system composed of all possible positions $\boldsymbol{x}$ and momenta $\boldsymbol{v}$, the probability of particles distribution of a fluid is f. f corresponds to the number of particles dN at a time t in a small element $d^3\boldsymbol{x}d^3\boldsymbol{v}$ centered in $(\boldsymbol{x}, \boldsymbol{v})$. If a system is composed of different components, there are N_i and f_i for each component i. The general equation which describes the evolution of f in the phase-space system is:

$$\partial_t f + \boldsymbol{v} \cdot \nabla_x f + \boldsymbol{a} \cdot \nabla_v f \ = \Omega(f, f) \tag{1}$$

Where the term $\boldsymbol{a}$ corresponds to the acceleration of particles induced by external forces. The term $\boldsymbol{v} \cdot \nabla_x f$ leads to the particles transportation. $\Omega(f, f)$ is the collision term explained afterwards.

The collision term $\Omega(f, f)$ represents the evolution of f over the phase-space system at each step of time Δt. The main model used is Bhatnagar-Gross-Krook (BGK) approximation (Bhatnagar et al. 1954) presented in (2) where the collision is driven by a non-equilibrium function. This non-equilibrium function depends on a maxwellian equilibrium distribution function called f_{eq}, at a given point in space and at a given temperature, and it occurs at a rate τ^{-1} related to the viscosity of the fluid.

$$\Omega(f, f) = \frac{1}{\tau\, \Delta t}\left(f_{eq} - f\right) \tag{2}$$

The function presented in Eq.1 is discretized in space and speed in a regular lattice. Resulting g, the particle distribution function discretized in the regular lattice. The evolution of the discrete distribution function of particle g in an element of space $\boldsymbol{x}$ for a discrete velocity e_α in time t following Boltzmann discrete equation is expressed in Eq.3 as:

$$g_\alpha(\boldsymbol{x} + e_\alpha \Delta t, t + \Delta t) = g_\alpha(\boldsymbol{x}, t) - \frac{1}{\tau}\Big(g_\alpha(x, t) - g_\alpha^{eq}(x, t)\Big) + F(x, t) \tag{3}$$

With F representing the external forces and τ the relaxation time given by BGK collision operator model (Bhatnagar et al. 1954). Referring to (Qian et al. 1992), the discrete scheme used for 2D simulations is the so-called D2Q9 model, which means 2 dimensions and 9 discrete velocities (Fig.1a). For the 3D simulations, the D3Q15 model is chosen (Wolf-Gladrow 2000), which corresponds to 3 dimensions and 15 discrete velocities (Fig.1b).

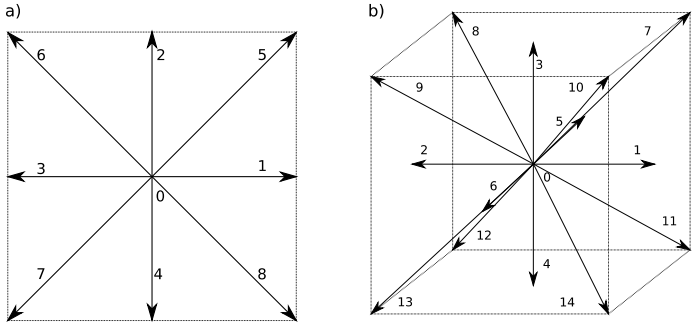

Figure 1: a) lattice scheme D2Q9, b) lattice Scheme D3Q15

For each element of space $\boldsymbol{x}$ the density ρ and macroscopic velocity u are determined for m the number of discrete velocities:

$$\rho(\boldsymbol{x},t) = \sum_{\alpha=0}^{m} g_\alpha(\boldsymbol{x},t) \tag{4}$$

$$u(\boldsymbol{x},t) = \frac{1}{\rho(\boldsymbol{x},t)} \sum_{\alpha=0}^{m} g_\alpha(\boldsymbol{x},t) \cdot e_\alpha \tag{5}$$

The equilibrium distribution function from the local Maxwellian equilibrium function at a time t (Bhatnagar et al. 1954):

$$g^{eq}(\boldsymbol{x},t) = \omega_\alpha \, \rho(\boldsymbol{x},t) \left(1 + \frac{3e_\alpha u}{c_s^2} + \frac{9(e_\alpha u)^2}{2c_s^4} - \frac{u^2}{2c_s^2}\right) \tag{6}$$

With c_s the sound speed in lattice and ω_α is the weight for a D2Q9 scheme (Qian et al. 1992):

$$\omega_\alpha = \begin{cases} 4/9, & \alpha = 0 \\ \dfrac{1}{9}, & \alpha = 1 \; to \; 4 \\ \dfrac{1}{36}, & \alpha = 5 \; to \; 8 \end{cases} \tag{7}$$

And the discrete velocities for a D2Q9 scheme (Qian et al. 1992):

$$e_\alpha = \begin{cases} (0,0), & \alpha = 0 \\ c\left(\cos\left[(\alpha-1)\dfrac{\pi}{2}\right], \sin\left[(\alpha-1)\dfrac{\pi}{2}\right]\right), & \alpha = 1 \; to \; 4 \\ \sqrt{2}c\left(\cos\left[(2\alpha-9)\dfrac{\pi}{4}\right], \sin\left[(2\alpha-9)\dfrac{\pi}{4}\right]\right), & \alpha = 5 \; to \; 8 \end{cases} \tag{8}$$

The lattice constant c is set as 1 such as $c = \frac{\Delta x}{\Delta t} = \frac{\Delta y}{\Delta t} = 1$ (Krüger et al. 2017).

1.2 Wetting simulation with Lattice Boltzmann Method

Wetting is the study of a liquid on a solid surrounded by gas (Fig.2) and can be modelled by a three body system composed by two fluids and one solid. For each fluid composing the system, a distribution function is needed. For the solid, a no-slip boundary condition has to be applied.

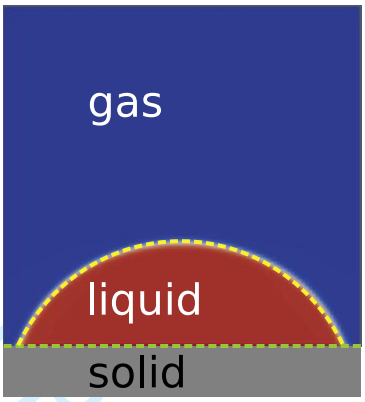

Figure 2: numerical system

To handle interactions at the interfaces, Eq.3 has to be adapted to wetting study. The external force $F(\boldsymbol{x}, t)$ used in Eq.3 includes two forces, the fluid-fluid force $F_{\sigma,\bar{\sigma}}$ applied at the fluid-fluid interface and the fluid-solid force $F_{ads,\sigma}$ applied at the fluid-solid interface. Because there are two fluids, the liquid σ and the gas $\bar{\sigma}$, each fluid has its own external force (Sukop and Thorne 2010) respectively F_{σ}, which correspond to Eq.9, and $F_{\bar{\sigma}}$.

$$F_{\sigma}(\boldsymbol{x}, t) = F_{\sigma\bar{\sigma}} + F_{ads,\sigma} \tag{9}$$

To model the fluid-fluid interaction, the pseudo-potential model of Shan Chen (SC) (Shan and Chen 1994) is chosen. Therefore, the first term in Eq.9 becomes Eq.10:

$$F_{\sigma\bar{\sigma}}(\boldsymbol{x}) = -G_{\sigma\bar{\sigma}}\psi_{\sigma}(\boldsymbol{x})c_s^2 \sum_{\alpha=1}^{e_\alpha} \omega_\alpha \psi_{\bar{\sigma}}(\boldsymbol{x} + e_\alpha)e_\alpha \tag{10}$$

With $G_{\sigma\bar{\sigma}}$ the coupling potential and $\psi_{\sigma}$the effective mass (Chen et al. 2014) expressed as:

$$\psi_{\sigma}(\boldsymbol{x}) = \rho_{0,\sigma}\left(1 - e^{-\frac{\rho_{\sigma}(\boldsymbol{x})}{\rho_{0,\sigma}}}\right) \tag{11}$$

The bulk density of the component σ is $\rho_{0,\sigma}$. The original form of effective mass is limited to low density ratio systems (up to 10) (Chen et al. 2014) so it cannot handle a density ratio of 1000 like water-air system. In this case, the models proposed in (Bao and Schaefer 2013; Chen et al. 2014) based on the equation of state of the system can be used.

Martys-Chen model (MC) (Martys and Chen 1996) is applied in order to control the fluid-solid interaction. Consequently, the second term in Eq.9 becomes:

$$F_{ads,\sigma}(\boldsymbol{x}) = -g_{ads,\sigma}\psi_{\sigma}(\boldsymbol{x})\sum_{\alpha=1}^{m}\omega_{\alpha}s(\boldsymbol{x}+e_{\alpha})e_{\alpha} \tag{12}$$

The term $g_{ads,\sigma}$ is the fluid-solid potential and $s(\boldsymbol{x}+e_{\alpha})$ is a geometrical parameter which returns 0 if the site $\boldsymbol{x}+e_{\alpha}$ is liquid and 1 if the site is solid. In addition, in order to get closer to a more classical wetting approaches, Sukop et al. (Sukop and Thorne 2010) proposed to express the interaction potential g_{ads} as a function of the wetting parameter θ_e by the following equation:

$$g_{ads,\sigma} = \frac{g_{\sigma\bar{\sigma}}}{2}cos\theta_e \tag{13}$$

θ_e is the equilibrium contact angle for a perfectly smooth and chemically homogeneous surface and it correspond to Young's contact angle.

1.3 Wetting Potential

The expression (Eq.13) of the fluid-solid force works for homogeneous surfaces but it can not handle a surface composed of two materials. For this case, there are two equilibrium contact angles, one for each material composing the surface. A model combining Martys-Chen model (Martys and Chen 1996) and Sukop et al. model (Sukop and Thorne 2010) and applicable to chemically textured substrates was not found in the literature. The authors have decided to modify MC model for the case of a substrate composed of different materials and to keep Eq.13 where the potential is function of the contact angle of the substrate.

Consequently, Eq.12 has to be expressed locally and thus take into account a surface with different fluid-solid interactions due to different materials. We propose therefore another expression of Eq.12 where the fluid-solid interaction potential is expressed locally:

$$F_{ads,\sigma}(\boldsymbol{x}) = -\psi_{\sigma}(\boldsymbol{x})\sum_{\alpha=1}^{m}\omega_{\alpha}\lambda_{\sigma,i}(\boldsymbol{x}+e_{\alpha})e_{\alpha} \tag{14}$$

With λ corresponding to the local fluid-solid interaction:

$$\lambda(\boldsymbol{x}+e_{\alpha}) = s(\boldsymbol{x}+e_{\alpha})\, g_{ads,\sigma,i}(\boldsymbol{x}+e_{\alpha}) \tag{15}$$

And

$$g_{ads,\sigma,i} = \frac{g_{\sigma\bar{\sigma}}}{2} cos\theta_{int,i} \tag{16}$$

Thus, the potential $g_{ads,\sigma,i}$ is function of the fluid-fluid potential $g_{\sigma\bar{\sigma}}$ and the intrinsic contact angle $\theta_{int,i}$ of each material bordering a fluid element (Fig.3). The intrinsic contact angle is the contact angle which describes the only static contact angle reached for a perfectly flat and chemically homogeneous surface for a material (Extrand 2006). For example, if we use the D2Q9 scheme in Fig.3 the fluid-solid interaction force (Eq.14) becomes:

$$\begin{cases} F_{ads,\sigma}(x_A) = \psi_\sigma(x_A) * g_{ads,\sigma,1} * (\omega_4 e_4 + \omega_7 e_7 + \omega_8 e_8) \\ F_{ads,\sigma}(x_B) = \psi(x_B) * \left[g_{ads,\sigma,1} * (\omega_4 e_4 + \omega_7 e_7) + g_{ads,\sigma,2} * (\omega_8 e_8)\right] \\ F_{ads,\sigma}(x_C) = \psi(x_C) * \left[g_{ads,\sigma,1} * (\omega_7 e_7) + g_{ads,\sigma,2} * (\omega_4 e_4 + \omega_8 e_8)\right] \\ F_{ads,\sigma}(x_D) = \psi(x_D) * g_{ads,\sigma,2} * (\omega_4 e_4 + \omega_7 e_7 + \omega_8 e_8) \end{cases} \tag{17}$$

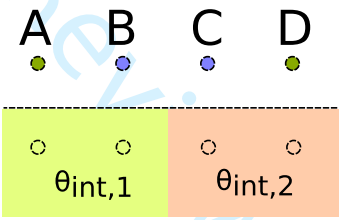

Figure 3: lattice fluid node A has every solid neighbor of the specie 1, B and C nodes are transition nodes, $\theta_{int,1}$ and $\theta_{int,2}$ are computed in $g_{ads,\sigma,i}$ and node D is only specie 2 dependent.

1.3 Lattice Boltzmann algorithm

The system is known at a time t and its state at $t + \Delta t$ is computed. This computational stage is performed by three successive steps. The first step computes physical quantities from the entering distribution functions and the velocities in each element of the lattice. Thus, Eq.4-5, Eq.10 and Eq.14-16 are computed, and correspond to the density, velocity and interaction forces at the interfaces. Then the second step which is the collision step (Eq.3 right part) consists of determining the new particle distribution in each element through the lattice. Finally the third step is related to the transfer of particles to neighbor elements (Eq.3 left part). And it is named the streaming step.

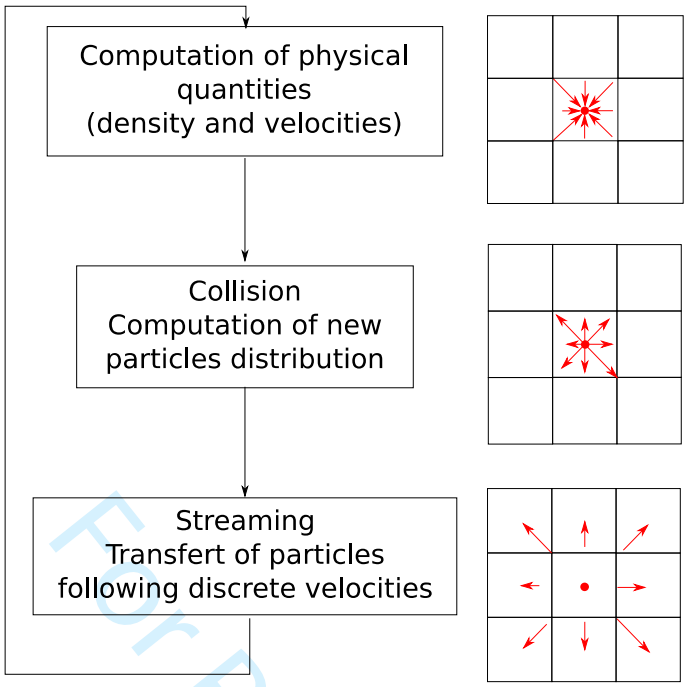

Figure 4: LBM algorithm scheme and the corresponding g_α (red arrows) in the lattice.

Boundary conditions are applied between collision step and streaming step. The boundary condition at wall is a no slip condition. The half-way bounce-back boundary condition scheme is used. It consists of returning particle transferred into the wall in their opposite direction in a single step of time (Fig.5) (Krüger et al. 2017).

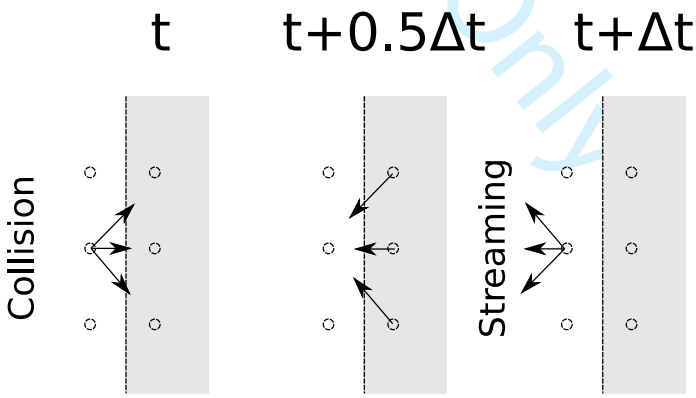

Figure 5: Half-way Bounce Back scheme

This algorithm is parallelizable, which makes it possible to perform computations on a Graphical Processing Unit (GPU). For this paper, the computations are performed on a NVIDA Quadro P5000 graphic board. Thus, the average time for a 2D simulation is 1 min for the 15,000 iterations to reach steady state. This time can increase for textured surfaces where it can take

up to 2 minutes to do 35,000 iterations before the final state. For 3D simulations, it takes around 3 min to reach final state in 20,000 iterations.

2. Numerical Validation

2.1 Validation of fluid-fluid interface

To validate the fluid-fluid interaction model (Eq.10), 2D and 3D tests are computed. These tests consist of verifying the geometrical convergence and volume conservation of a system at equilibrium composed of the liquid and the gas which were initially out of equilibrium. The equilibrium state of a liquid surrounded by gas is a spherical droplet (Laplace 1805) so that, to realize the non-equilibrium initial state, the shape of the liquid is imposed: squared for 2D simulation and cubic for 3D simulation. Then, LBM algorithm is computed up to the equilibrium state and computations are performed with single precision for more efficient time saving thanks to GPU parallelization.

Therefore, the numerical simulations carried out to model the validation test is in a lattice of 200*200 lattice unit (lu) in 2D and 200*200*200 lu in 3D. The liquid is initially a square with a side size of 100 lu for 2D (Fig.6a) and is a cube with a side size of 100 lu (Fig.6c) for 3D. The final state is presented in Fig.6b and in Fig.6d. In addition, the shape and the volume loss are characterized in Fig.7.

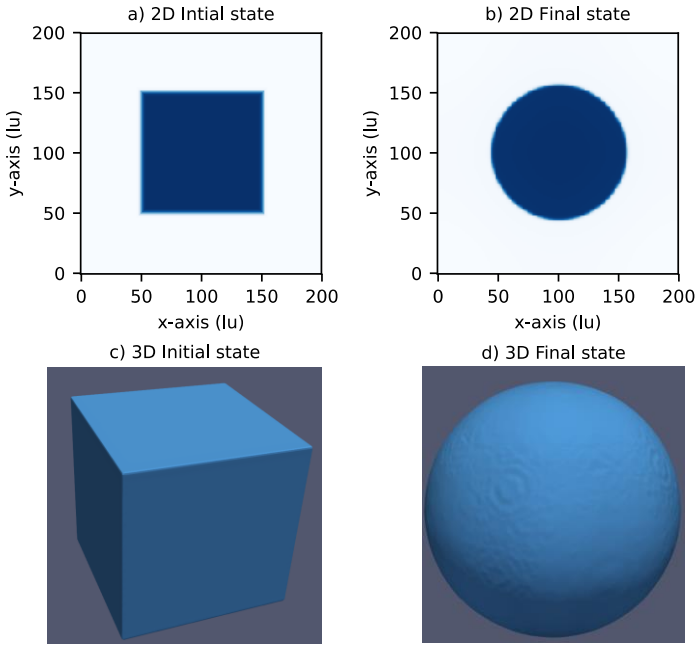

Figure 6: 2D and 3D simulations of a droplet surrounded by gas

The root mean square roundness deviation parameter presented in Eq.18 (ΔR_{rms}) (ISO 12181-1:2011) is used to quantify the circularity of the simulated droplet at equilibrium state.

$$\Delta R_{rms} = \sqrt{\frac{1}{2\pi}\int_0^{2\pi} \Delta R_i^2 \, d\theta} \tag{18}$$

With ΔR_i the difference between the mean radius and the local radius: $R_{mean} - R_{local}$.

The measurements of ΔR_{rms} show that the circular shape of the final droplets in 2D and 3D is achieved since $\Delta R_{rms} = 0.08$ for 2D simulation and $\Delta R_{rms} = 0.02$ for 3D simulation. Hence, for both simulations, the loss of volume is lower than 5% (2% loss for 2D and 4% for 3D). To conclude, the fluid-fluid interaction model can be validated for the two configurations of the present study.

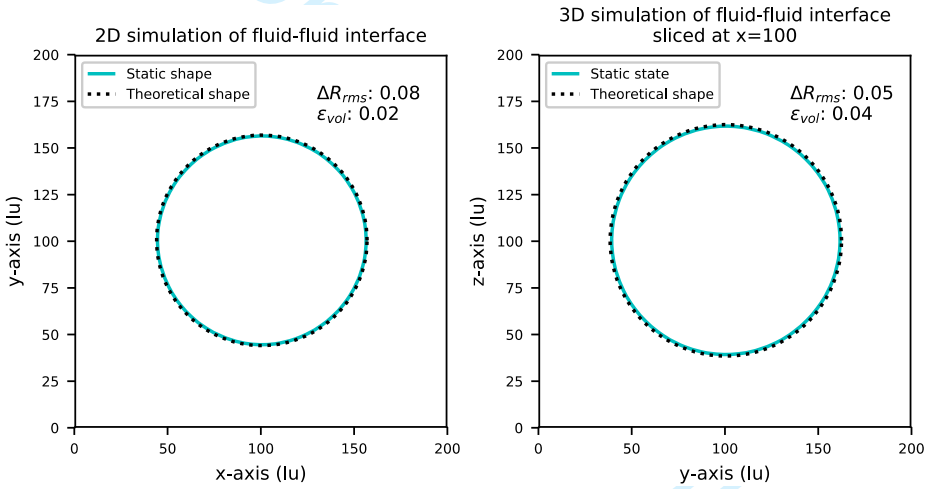

Figure 7: Circularity and volume conservation in 2D and 3D simulation and comparison to optimized shape (Laplace 1805).

2.2 Validation of fluid-solid interface

We now propose to validate the fluid-solid interaction model (Eq.14-16) by a numerical test of the sessile test under Young's law condition (Young 1805). The sessile test is commonly used for determine the wetting properties of a surface. A liquid spherical droplet surrounded by gas is dropped tangentially to the interface without initial speed. The final state of the simulation is supposed to give the equilibrium contact angle of the surface.

For 2D test, the size of the lattice is 500*500 lu and the droplet has a radius of 100 lu. In 3D the system has a lattice of 250*250*250 lu and the droplet has a radius of 50 lu. A wide range of material is tested and presented in Table.1. The variable which changes at every simulation is

the intrinsic contact angle of the surface and it corresponds to its Young contact angle. This modification occurs in Eq.14-16. The contact angles tested vary from 67° to 112° depending on the tested material in Table 1. For both 2D and 3D simulations initial states and final states on PA6.6 and PDMS are exposed Fig.8. Contact angles resulting from the simulation are plotted in Fig.9 as a function of the intrinsic contact angle applied to the substrate. In addition, in order to measure the correlation between the simulated and the inputted contact angles, the r-squared parameter is computed with the following equation (Eq.19):

$$R^2 = 1 - \frac{\sum(y_i - \hat{y})^2}{\sum(y_i - \bar{y})^2} \tag{19}$$

With y_i the simulated contact angle, $\hat{y}$ the intrinsic contact angle of the surface and $\bar{y}$ the mean value of the contact angle.

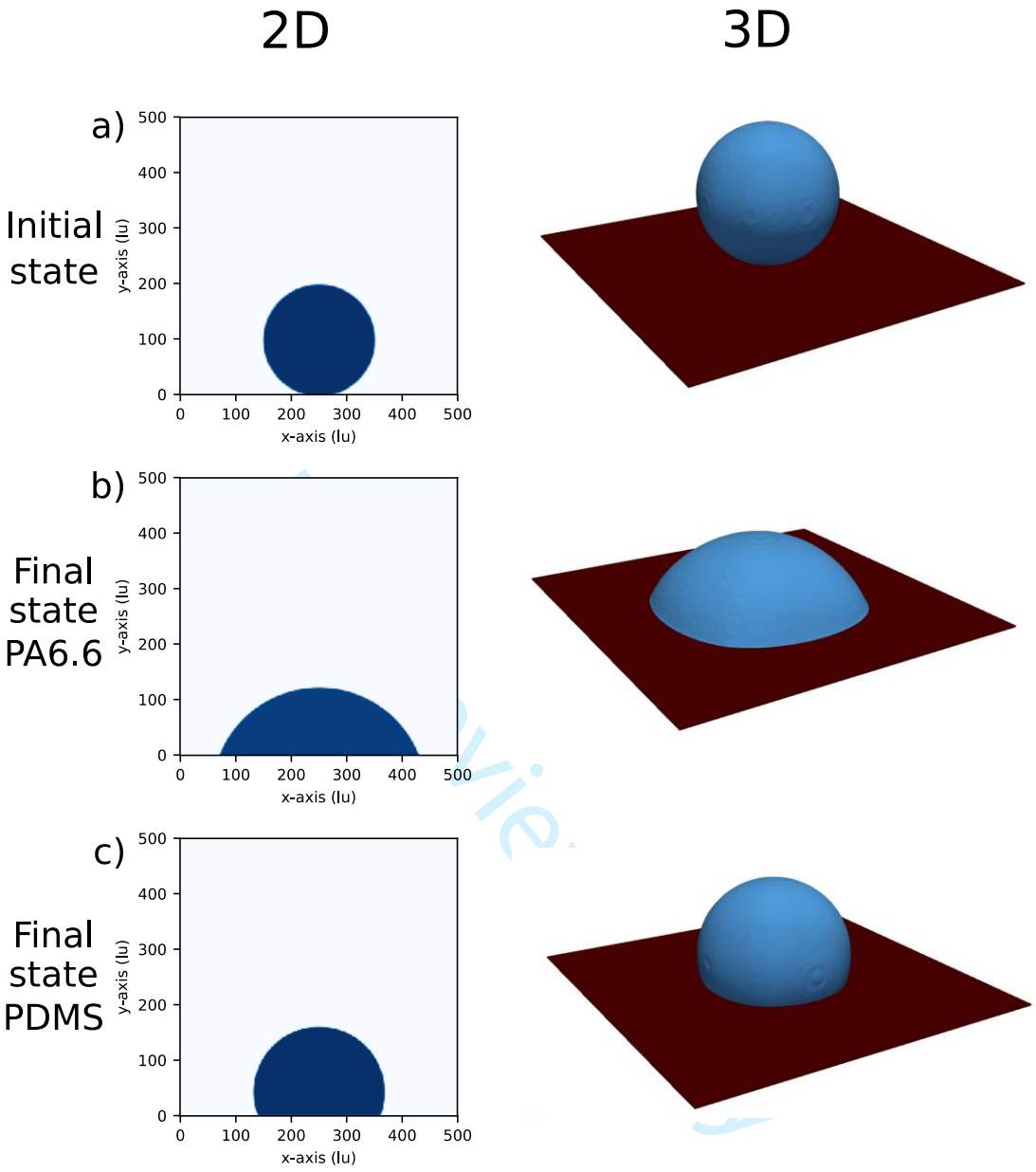

Figure 8: a) initial state for 2D and 3D simulation, b) 2D final state on PA6.6 for 2D and 3D simulation, c) 2D final state on PDMS for 2D and 3D simulation.

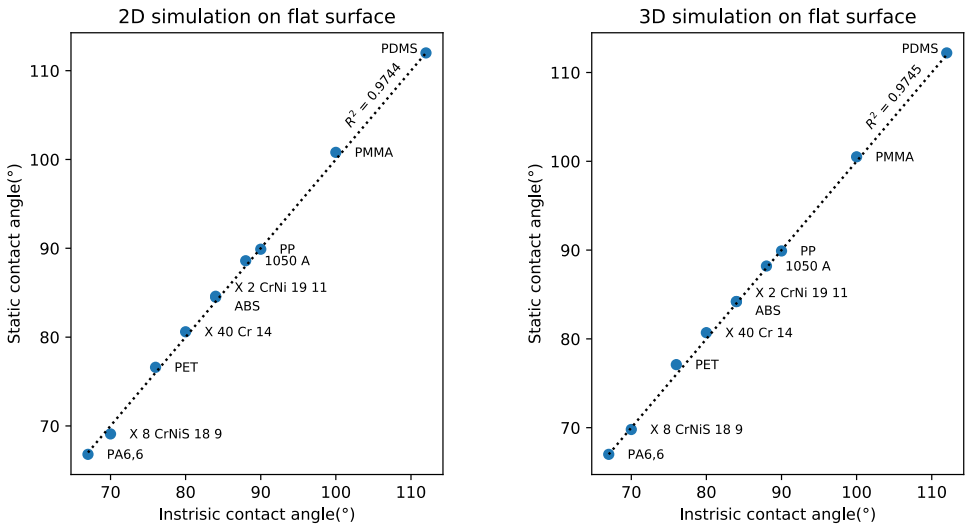

Figure 9: Validation results for 2D and 3D simulations

Materials	References	Intrinsic contact angle (°)
Polyamide	PA6,6	67
Stainless Steel	X 8 CrNiS 18 9	70
Polyethylene Terephthalate	PET	76
Stainless Steel	X 40 Cr 14	80
Acrylonitrile Butadiene Styrene	ABS	84
Stainless Steel	X 2 CrNi 19 11	84
Aluminium alloy 1050	1050 A	88
Polypropylene	PP	90
Polymethyl Methacrylate	PMMA	100
Polydimethylsiloxane	PDMS	112

Table 1: Solid simulated

The measurement of the r-squared parameters for 2D and 3D simulations show that the simulation are resulting a contact angle similar to the inputted one with a r-squared value

higher than 0.974 in both cases. To conclude, the fluid-solid interaction model can be validated for the two configurations of the present study.

3. 2D simulation on chemically textured surfaces

It is now proposed to simulate wetting on chemically textured surfaces using the Eq.14 and to compare the results with theoretical wetting models. Different materials have been tested previously (section 2.2) and, in order to obtain the greatest difference between the contact angles, two are sectioned: PA6.6 (67°) and PDMS (112°). Thus, substrate with two materials is numerically generated (Fig.10), dark-gray is PDMS and light-gray is PA6.6. Four configurations are tested for different size of domains c = 10, 20, 40 and 100 lu (Fig.10). The size of the lattice is 300*300 lu and the initial shape of the liquid is a circle with a radius of 75 lu where the initial position is initially tangent to the surface.

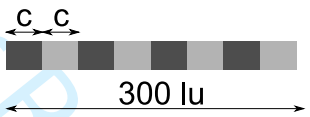

Figure 10: Scheme of generated substrate.

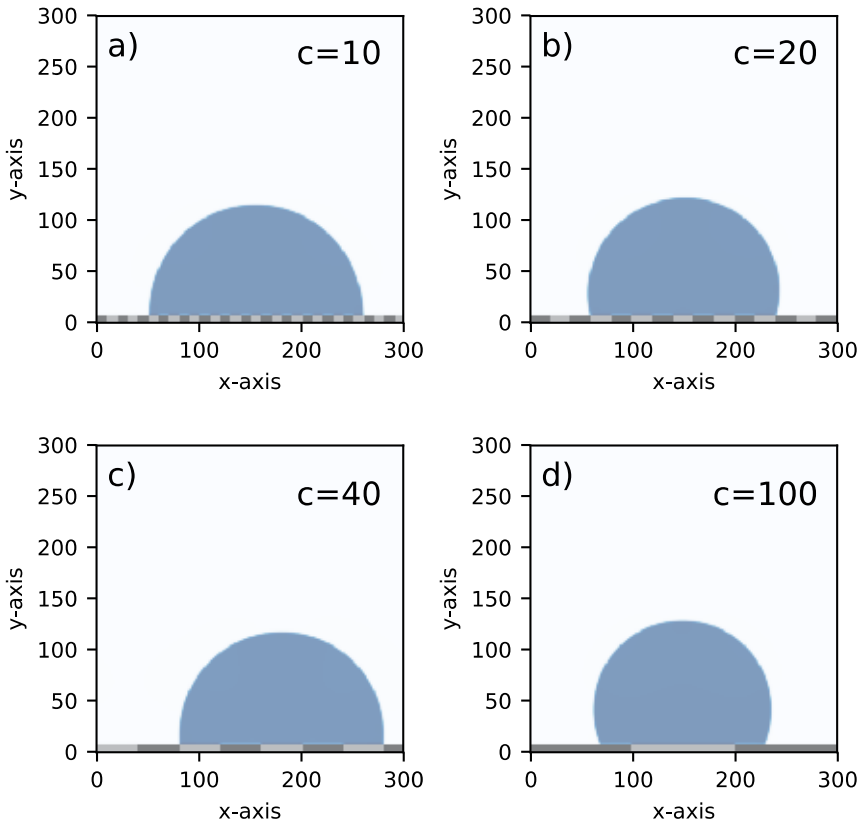

Figure 11: 2D simulation of sessile test on chemically textured surface.

The contact angle measured for the final state of each simulation is presented in Table.2 and is always comprised between the specific contact angles of the chosen materials. Table 2 also presents a comparison between the measured values and the theoretical values calculated with Eq.20 , the Cassie model (Cassie and Baxter 1944).

$$cos\theta_e = f_1 \cos\theta_1 + f_2 cos\theta_2 \quad (20)$$

With f_1 the PA6.6 surface fraction, f_2 de PDMS surface fraction, θ_1 the contact angle of PA6.6 and θ_2 the contact angle of PDMS.

c (lu)	f1	f2	θ_e (Cassie)	θ_e (Simulated)
10	0.52	0.48	88.5	88
20	0.56	0.44	87.1	99
40	0.6	0.4	85.1	90
100	0.67	0.33	82.2	113

Table 2: Numerical results for 2D simulation

The differences between the Cassie model and the numerical simulations (Table 2) tend to show that Cassie model is less and less verified by increasing the size of the domains c. On the contrary, when the size c is the largest (Fig.10d), the simulated contact angle is equal to the intrinsic contact angle of the material under the triple line. Assuming that the wetting phenomenon depends on the positions of the triple line, it is notable that for c = 10, 20 and 40 triple lines are stuck at the border between the PA6.6 and the PDMS. These positions of the triple may explain that the final contact angle is between 67° and 112°. Furthermore, the phenomenon modeled when $c = 100$ has been experimentally observed by Gao and McCarthy (Gao and McCarthy 2007) and Extrand (Extrand 2016). The validity of the theoretical approaches of Cassie (Cassie and Baxter 1944) and Gao (Gao and McCarthy 2007) are questioned and deserves further investigations.

4. 3D simulation on chemically textured surfaces

It has been shown that the simulation of wetting in 2D systems gives interesting results that challenge theoretical models. Hence, it is necessary to look numerically at the behavior of a droplet on a chemically textured surface to see if in 3D there are still deviations from theoretical approaches. We therefore propose to simulate in 3D the wetting on chemically textured surfaces. The systems simulated have a size 250*250*250 lu with a spherical droplet of 75 lu radius. A sessile test is numerically performed so that, at the initial state, the droplet is tangent

to the surface without initial speed. As presented in Fig.9, surfaces are made of two different materials, PA6.6 and PDMS. Four different simulations are shown in Fig.12. The final state is achieved for a static droplet and then, geometrical properties measured on the droplet simulated are presented in Table3. Cases A, B and C are first compared because they have similar setup with different size of chemically textured surface. Those cases permit to observe the effect of the size of the textures on the wetting properties of the surface. The surface in case A has the smallest band width ($c = 10$) and the case C has the largest band width ($c = 50$). In addition, for case C and case D the surface is the same but the droplet is initially centered on the opposite domain. It shows the influence of the chemical properties of the substrate on the initial contact area. Case C is for the hydrophilic initial contact area and case D is for the hydrophobic initial contact area.

The parameters used to compare wetting on different surfaces are:

- the size of the spreading measured by the wet area of the surface,
- the ratio of the wet area on hydrophilic domain over the wet area on hydrophobic domain (A_{hi}/A_{ho}),
- the number of hydrophilic domain in contact with the droplet N_{hi},
- the ΔR_{rms} parameter (Eq.18),
- the maximum and minimum contact angle measured.

Cases	Band width c (lu)	Wet area (lu^2)	$\frac{A_{hi}}{A_{ho}}$	N_{hi}	ΔR_{rms}	θ_{max} (°)	θ_{min} (°)
A	10	11726	1.16	6	2.48	113	67
B	25	10602	1.47	2	7.78	113	68
C	50	15004	1.93	2	9.61	112	66
D	50	10740	2.19	1	10.74	113	66

Table 3: Geometrical properties of the droplet simulated in fig.12

For each simulation, a wide range of angles is measured, but the extreme angles correspond in each case to the angles of the PA6.6 and PDMS.

As expected for cases A, B and C, the ratio A_{hi}/A_{ho} is higher than 1, which implies that the wetting is favored on hydrophilic area. In addition, it is observed that the ratio increase with the increase of the size of the band. Smaller are domains, smaller is the ratio. The ΔR_{rms} parameter is small for the case A and increase witch cases B and C.

For cases C and D, the wetting is different even if the textured surfaces are the same, which shows that the initial position of the droplet influences its static state. The transition

hydrophobic to hydrophilic or opposite occurs for a spreading through x-axis, y-axis in not bounded by a change of material so y-axis is homogeneous. Both droplets for cases C and D have a transition but in the first case (C), the transition is from hydrophobic to hydrophilic and for the second case (D) transition is hydrophilic to hydrophobic. It is observed that the transition from hydrophobic to hydrophilic is favored against the transition from hydrophilic to hydrophobic.

It is stated that the size of the bands is related to circularity and the better the circularity, the smaller the bands are. Therefore, wetting has a higher anisotropy for a larger chemically textured domain and, on the contrary, for small bands, seems to reduce the spreading deviations and is closer to Cassie's theory. In addition, if the initial domain is hydrophilic, the transition during spreading from a hydrophilic to a hydrophobic surface appears to force the droplet to spread only in the hydrophilic domain. Further, if the droplet is initially on a hydrophobic surface it will also leak from the hydrophobic domain into the hydrophilic domain and spread there.

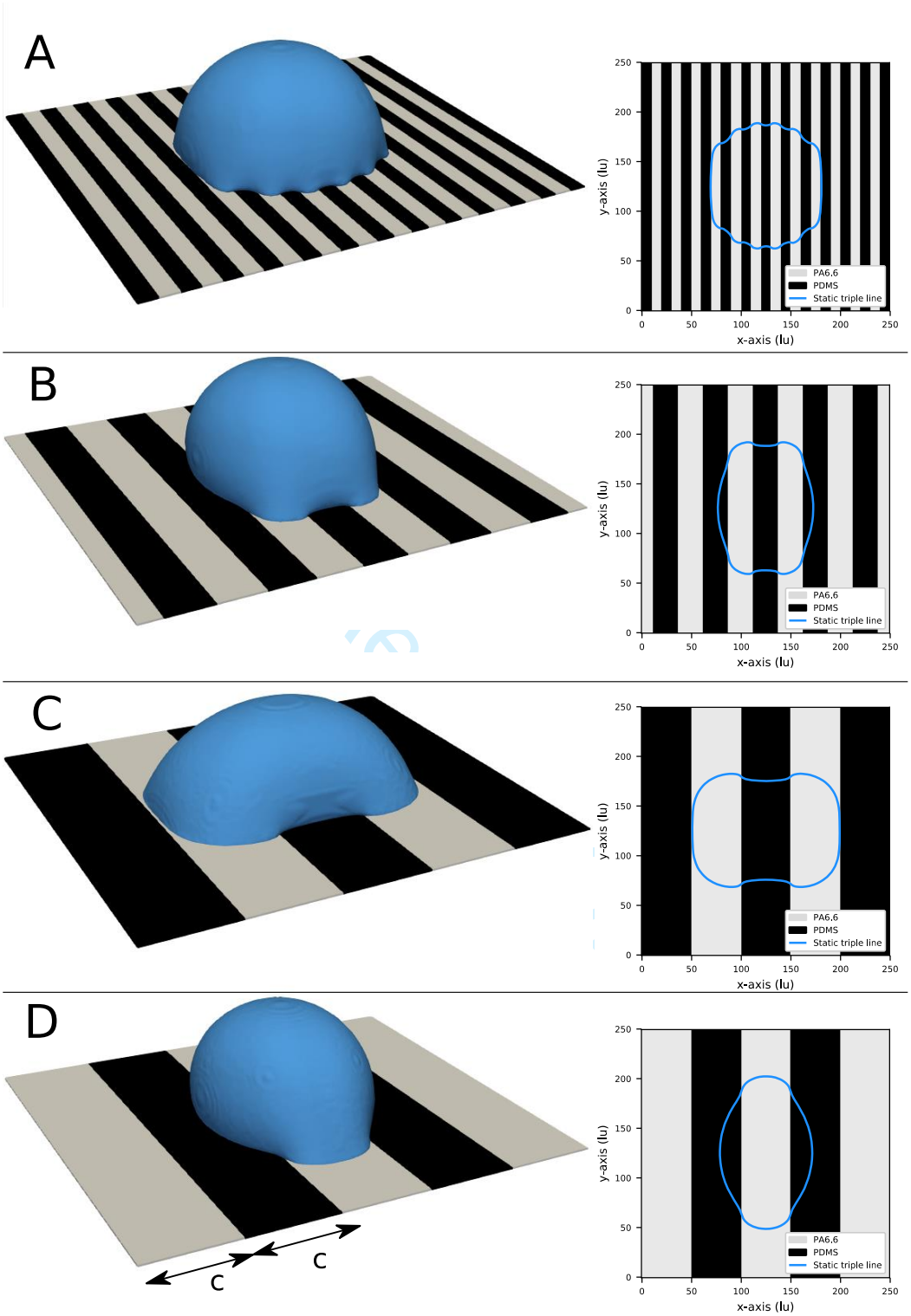

Figure 12: 3D simulations on chemically textured surfaces

5. Conclusion

A numerical tool has been developed in order to simulate wetting on chemically textured surfaces. This tool is based on lattice Boltzmann method which allows the use of local interactions between fluids and solids. For this reason, chemically textured surfaces are easier to implement in the method. Because wetting is a three body system, two fluids are simulated, the liquid and the gas, and in contact with a solid. Initially, the Martys-Chen model (Martys and Chen 1996) combined with the Sukop et al. model (Sukop and Thorne 2010) was used, but a modification was proposed in order to be able to simulate wetting on surfaces with different chemistries while keeping their intrinsic contact angle as a simulation parameter.

The fluid-fluid interaction model is verified by the simulation of the perfect equilibrium state for a two-fluid system. Volume and shape are verified and validated. Then fluid-solid interaction model has been verified by the simulation of sessile tests for different chemically homogeneous surfaces. For the range of materials tested as substrates, the final state contact angles simulated are corresponding to the contact angle initially imposed to the simulation.

2D and 3D simulations on chemically textured surfaces are tested. It is observed that for 2D simulations, some theoretical approaches and the simulations have different results. The Cassie (Cassie and Baxter 1944) model is approached for small band size textured substrates and models of Extrand (Extrand 2003) and Gao (Gao and McCarthy 2007) are more effective for larger band textured surfaces. Thus, through simulation and by taking into account the chosen interaction model, it has been shown that simulation and theoretical approaches can be compared in order to better understand wetting.

A high anisotropy of wetting is observed for 3D simulations. It has been shown that initial contact areas properties have an influence on droplets' spread so that on their final state. It is observed that the hydrophilic domain promotes spreading compared to the hydrophobic where spreading is refrained. According to the observations and simulations on chemically textured surfaces, the size of each domain has an effect on the spreading and, by extension, to the static state. It is observed that the transition from hydrophobic to hydrophilic surface is mainly driving the spreading and, at the opposite, the transition from hydrophilic to hydrophobic is blocking the spreading. More in-depth studies are ongoing to understand these exposed phenomena.

Acknowledgments

This work is supported by LABEX MANUTECH-SISE (ANR-10-LABX-0075) of Université de Lyon, within the program Investissements d'Avenir (ANR-11-IDEX-0007) operated by the French National Research Agency (ANR) and by l'EQUIPEX MANUTECH-USD (ANR-10-EQPX-36-01).

References

Bao J, Schaefer L (2013) Lattice Boltzmann equation model for multi-component multi-phase flow with high density ratios. Appl Math Model 37:1860–1871. https://doi.org/10.1016/j.apm.2012.04.048

Barthlott W, Mail M, Bhushan B, Koch K (2017) Plant Surfaces: Structures and Functions for Biomimetic Innovations. Nano-Micro Lett 9:23. https://doi.org/10.1007/s40820-016-0125-1

Belaud V, Valette S, Stremsdoerfer G, et al (2015) Wettability versus roughness: Multi-scales approach. Tribol Int 82:343–349. https://doi.org/10.1016/j.triboint.2014.07.002

Benzi R, Succi S, Vergassola M (1992) The lattice Boltzmann equation: theory and applications. Phys Rep 222:145–197. https://doi.org/10.1016/0370-1573(92)90090-M

Bhatnagar PL, Gross EP, Krook M (1954) A Model for Collision Processes in Gases. I. Small Amplitude Processes in Charged and Neutral One-Component Systems. Phys Rev 94:511–525. https://doi.org/10.1103/PhysRev.94.511

Bizi-Bandoki P, Benayoun S, Valette S, et al (2011) Modifications of roughness and wettability properties of metals induced by femtosecond laser treatment. Appl Surf Sci 257:5213–5218. https://doi.org/10.1016/j.apsusc.2010.12.089

Bruchon J, Liu Y, Moulin N (2018) Finite element setting for fluid flow simulations with natural enforcement of the triple junction equilibrium. Comput Fluids 171:103–121. https://doi.org/10.1016/j.compfluid.2018.06.007

Cahn JW, Hilliard JE (1958) Free Energy of a Nonuniform System. I. Interfacial Free Energy. J Chem Phys 28:258–267. https://doi.org/10.1063/1.1744102

Cassie ABD, Baxter S (1944) Wettability of porous surfaces. Trans Faraday Soc 40:546–551. https://doi.org/10.1039/TF9444000546

Chen L, Kang Q, Mu Y, et al (2014) A critical review of the pseudopotential multiphase lattice Boltzmann model: Methods and applications. Int J Heat Mass Transf 76:210–236. https://doi.org/10.1016/j.ijheatmasstransfer.2014.04.032

Choi W, Tuteja A, Mabry JM, et al (2009) A modified Cassie–Baxter relationship to explain contact angle hysteresis and anisotropy on non-wetting textured surfaces. J Colloid Interface Sci 339:208–216. https://doi.org/10.1016/j.jcis.2009.07.027

de Gennes PG (1985) Wetting: statics and dynamics. Rev Mod Phys 57:827–863. https://doi.org/10.1103/RevModPhys.57.827

Divin-Mariotti S, Amieux P, Pascale-Hamri A, et al (2019) Effects of micro-knurling and femtosecond laser micro texturing on aluminum long-term surface wettability. Appl Surf Sci 479:344–350. https://doi.org/10.1016/j.apsusc.2019.02.025

Dubov AL, Teisseire J, Barthel E (2012) Elastic Instability and Contact Angles on Hydrophobic Surfaces with Periodic Textures. EPL - Europhys Lett 97:26003. https://doi.org/10.1209/095-5075/97/97/26003

Erbil HY (2006) Solid and liquid interfaces. Blackwell Publishing, Oxford

Erbil HY (2014) The debate on the dependence of apparent contact angles on drop contact area or three-phase contact line: A review. Surf Sci Rep 69:325–365. https://doi.org/10.1016/j.surfrep.2014.09.001

Extrand CW (2003) Contact Angles and Hysteresis on Surfaces with Chemically Heterogeneous Islands. Langmuir 19:3793–3796. https://doi.org/10.1021/la0268350

Extrand CW (2006) Designing for Optimum Liquid Repellency. Langmuir 22:1711–1714. https://doi.org/10.1021/la052540l

Extrand CW (2016) Origins of Wetting. Langmuir 32:7697–7706. https://doi.org/10.1021/acs.langmuir.6b01935

Gao L, McCarthy TJ (2007) How Wenzel and Cassie Were Wrong. Langmuir 23:3762–3765. https://doi.org/10.1021/la062634a

Ge D, Yang L, Zhang Y, et al (2014) Transparent and Superamphiphobic Surfaces from One-Step Spray Coating of Stringed Silica Nanoparticle/Sol Solutions. Part Part Syst Charact 31:763–770. https://doi.org/10.1002/ppsc.201300382

Gong W, Yan Y, Chen S, Giddings D (2017) Numerical Study of Wetting Transitions on Biomimetic Surfaces Using a Lattice Boltzmann Approach with Large Density Ratio. J Bionic Eng 14:486–496. https://doi.org/10.1016/S1672-6529(16)60414-6

Huang H, Thorne DT, Schaap MG, Sukop MC (2007) Proposed approximation for contact angles in Shan-and-Chen-type multicomponent multiphase lattice Boltzmann models. Phys Rev E 76:066701. https://doi.org/10.1103/PhysRevE.76.066701

Jiang T, Peng Z, Wu W, et al (2014) Gas sensing using hierarchical micro/nanostructures of Morpho butterfly scales. Sens Actuators Phys 213:63–69. https://doi.org/10.1016/j.sna.2014.04.002

Krüger T, Kusumaatmaja H, Kuzmin A, et al (2017) The Lattice Boltzmann Method: Principles and Practice. Springer International Publishing

Kubiak K, Wilson M, Mathia T, Carras S (2011) Dynamics of Contact Line Motion During the Wetting of Rough Surfaces and Correlation With Topographical Surface Parameters. Scanning 33:370–7

Laplace PS de (1805) Oeuvres complètes de Laplace. p 392

Latthe SS, Sutar RS, Kodag VS, et al (2019) Self – cleaning superhydrophobic coatings: Potential industrial applications. Prog Org Coat 128:52–58. https://doi.org/10.1016/j.porgcoat.2018.12.008

Martys NS, Chen H (1996) Simulation of multicomponent fluids in complex three-dimensional geometries by the lattice Boltzmann method. Phys Rev E 53:743–750. https://doi.org/10.1103/PhysRevE.53.743

Mielczarek WS, Obaje EA, Bachmann TT, Kersaudy-Kerhoas M (2016) Microfluidic blood plasma separation for medical diagnostics: is it worth it? Lab Chip 16:3441–3448. https://doi.org/10.1039/c6lc00833j

Niu S, Li B, Mu Z, et al (2015) Excellent Structure-Based Multifunction of Morpho Butterfly Wings: A Review. J Bionic Eng 12:170–189. https://doi.org/10.1016/S1672-6529(14)60111-6

Pionnier N, Vera J, Contraires E, et al (2018) The effect of the orientation and the height of periodic sub-micrometric texturing on dropwise condensation. J Colloid Interface Sci 526:184–193. https://doi.org/10.1016/j.jcis.2018.04.043

Pravinraj T, Patrikar R (2017) Modelling and investigation of partial wetting surfaces for drop dynamics using lattice Boltzmann method. Appl Surf Sci 409:214–222. https://doi.org/10.1016/j.apsusc.2017.02.242

Qian YH, D'Humières D, Lallemand P (1992) Lattice BGK Models for Navier-Stokes Equation. Europhys Lett EPL 17:479–484. https://doi.org/10.1209/0295-5075/17/6/001

Renardy M, Renardy Y, Li J (2001) Numerical Simulation of Moving Contact Line Problems Using a Volume-of-Fluid Method. J Comput Phys 171:243–263. https://doi.org/10.1006/jcph.2001.6785

Shan X, Chen H (1994) Simulation of nonideal gases and liquid-gas phase transitions by the lattice Boltzmann equation. Phys Rev E 49:2941–2948. https://doi.org/10.1103/PhysRevE.49.2941

Shin B, Ha J, Lee M, et al (2018) Hygrobot: A self-locomotive ratcheted actuator powered by environmental humidity. Sci Robot 3:. https://doi.org/10.1126/scirobotics.aar2629

Solomenko Z, Spelt PDM, Alix P (2017) A level-set method for large-scale simulations of three-dimensional flows with moving contact lines. J Comput Phys 348:151–170. https://doi.org/10.1016/j.jcp.2017.07.011

Spelt PDM (2005) A level-set approach for simulations of flows with multiple moving contact lines with hysteresis. J Comput Phys 207:389–404. https://doi.org/10.1016/j.jcp.2005.01.016

Sui Y, Ding H, Spelt PDM (2014) Numerical Simulations of Flows with Moving Contact Lines. Annu Rev Fluid Mech 46:97–119. https://doi.org/10.1146/annurev-fluid-010313-141338

Sukop MC, Thorne DT (2010) Lattice Boltzmann Modeling: An Introduction for Geoscientists and Engineers, 1st edn. Springer Publishing Company, Incorporated

Sussman M, Almgren AS, Bell JB, et al (1999) An Adaptive Level Set Approach for Incompressible Two-Phase Flows. J Comput Phys 148:81–124. https://doi.org/10.1006/jcph.1998.6106

Unverdi SO, Tryggvason G (1992) A front-tracking method for viscous, incompressible, multi-fluid flows. J Comput Phys 100:25–37. https://doi.org/10.1016/0021-9991(92)90307-K

Vera J, Contraires E, Brulez A-C, et al (2017) Wetting of polymer melts on coated and uncoated steel surfaces. Appl Surf Sci 410:87–98. https://doi.org/10.1016/j.apsusc.2017.02.067

Wenzel RN (1936) RESISTANCE OF SOLID SURFACES TO WETTING BY WATER. Ind Eng Chem 28:988–994. https://doi.org/10.1021/ie50320a024

Wolf-Gladrow D (2000) Lattice-Gas Cellular Automata and Lattice Boltzmann Models - An Introduction. Springer, Berlin

Young T (1805) An essay on the cohesion of fluids. Philos Trans Roy Soc Lond

Yue P, Feng JJ (2011) Wall energy relaxation in the Cahn–Hilliard model for moving contact lines. Phys Fluids 23:012106. https://doi.org/10.1063/1.3541806

Zhang D, Luo Y, Li X, Chen H (2011) Numerical simulation and experimental study of drag-reducing surface of a real shark skin. J Hydrodyn Ser B 23:204–211. https://doi.org/10.1016/S1001-6058(10)60105-9

Zhang J, Borg MK, Reese JM (2017) Multiscale simulation of dynamic wetting. Int J Heat Mass Transf 115:886–896. https://doi.org/10.1016/j.ijheatmasstransfer.2017.07.034

Zhang M, Feng S, Wang L, Zheng Y (2016) Lotus effect in wetting and self-cleaning. Biotribology 5:31–43. https://doi.org/10.1016/j.biotri.2015.08.002

ISO 12181-1:2011, Geometrical product specifications (GPS) — Roundness — Part 1: Vocabulary and parameters of roundness. https://www.iso.org/obp/ui/#iso:std:iso:12181:-1:ed-1:v1:fr. Accessed 10 Dec 2019